ELSEVIER

Surface Science 475 (2001) 47–60

SURFACE SCIENCE

www.elsevier.nl/locate/susc

A molecular orbital study of surface–adsorbate interactions during the oxidation of CO on the Pt(1 1 1) surface

Wingfield V. Glassey *, Roald Hoffmann

Department of Chemistry and Chemical Biology, Cornell University, Ithaca, NY 14853-1301, USA

Received 15 September 2000; accepted for publication 20 November 2000

Abstract

A Langmuir–Hinshelwood type pathway for the oxidation of CO on the Pt(1 1 1) surface is analysed within a tight binding scheme based on the extended Hückel method. A partitioning of the total electronic energy serves to highlight both CO and O derived contributions to the reaction barrier, the extent to which the surface mediates interactions between the adsorbates and the roles of the individual CO and O orbitals in OC–O bond formation.

The reaction barrier is interpreted to be the result of a surface-mediated coactivation of CO and O on the surface. In the initial stages of OC–O bond formation a ''side-on'' donation of electron density from the p-orbitals on O to the empty CO(2π) orbitals on CO occurs. The transition from reactants to products is characterized by the formation of a carboxylate (CO_2^-) moiety on the surface. The role of the O s and p orbitals in OC–O bonding is discussed.

Keywords: Carbon monoxide; Chemisorption; Oxidation; Catalysis; Adsorption kinetics

1. Introduction

The removal of toxic CO emissions from automotive exhaust gases via catalytic oxidation is a process of prime environmental importance, yet there is still much to be learned about the nature of the reaction between chemisorbed CO and O on surfaces.

Above room temperature, CO oxidation is believed to proceed via a Langmuir–Hinshelwood mechanism (Scheme 1) [1,2]. In this study we construct a molecular orbital based picture of the evolution of both surface–adsorbate and adsorbate–adsorbate bonding along the reaction coordinate for the reaction between CO and O on the Pt(1 1 1) surface. Our analysis of the electronic structure changes accompanying the reaction utilizes Hamilton population analysis – a partitioning of the total electronic energy – within a tight-binding formalism based on the extended Hückel method [3].

To date most theoretical accounts of CO oxidation have focussed on the energetics of the reaction. Indeed with the modern tools of computational chemistry, this can be done quite reliably. Our aim is to construct a qualitative model of orbital interactions along the reaction coordinate, adding to

* Corresponding author. Present address: Department of Chemistry, Lewis and Clark College, 0615 SW Palatine Hill Road, Portland, OR 97219, USA. Tel.: +1-503-768-7534; fax: +1-503-768-7369.

E-mail address: glassey@lclark.edu (W.V. Glassey).

0039-6028/01/$ - see front matter
PII: S0039-6028(00)01062-1

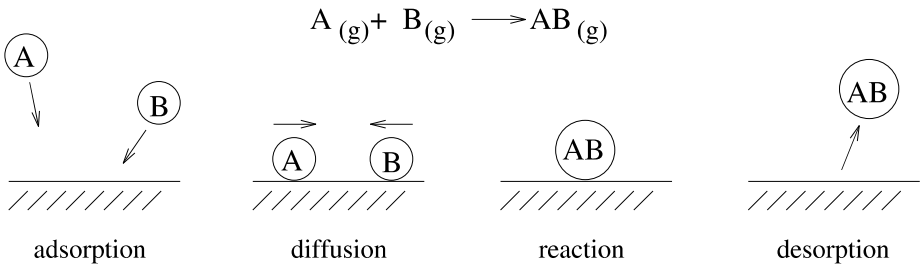

Scheme 1.

our physical and chemical understanding of the reaction.

The computational transparency of a one-electron tight binding scheme affords us the opportunity to investigate aspects of the reaction that cannot be easily addressed with other more computationally intensive methods. In particular we investigate the extent to which surface–adsorbate interactions can be localized on the surface and we provide an in-depth analysis of the extent to which the surface mediates the interactions between the adsorbates.

A recent STM study of CO oxidation proposed the reaction between chemisorbed CO and O at the boundaries of CO and O "islands" on the surface [1]. Nonetheless we choose to study the reaction between ordered, periodic arrays of CO and O chemisorbed on the surface. We believe that in order to fully understand the reaction between chemisorbed CO and O at the edges of adsorbate islands – which potentially involves absorbates that are not associated with particular surface sites – it is first necessary to understand the reaction between adsorbates that are, at least initially, associated with specific surface sites.

2. Computational methodology

In our molecular orbital based analysis of the reaction between CO and O we analyze the electronic structure of the set of eight atomic configurations calculated by Alavi et al. [4] in their ab initio DFT study of CO oxidation on Pt(1 1 1). These configurations are subsequently referred to as reaction "frames" and are illustrated in Fig. 1.

Each frame in Fig. 1 results from the relaxation of CO, O and the Pt atoms belonging to the surface layer for a given (fixed) distance between the carbon atom of the chemisorbed CO molecules and the nearest-neighbour O chemisorbed on the surface. Thus the reaction is modelled as a "linear transit" with respect to the length of the newly formed OC–O bond.

As we scan through the reaction frames in Fig. 1, our interest is naturally focussed on the interactions between CO and the surface, O and the surface, and the interactions between chemisorbed CO and O. With this in mind it makes chemical sense to sub-divide the chemisorption system into three geometric fragments, the CO molecule, the

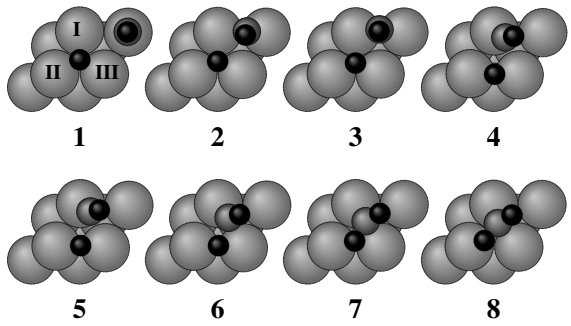

Fig. 1. The sequence of eight frames used by Alavi et al. to characterize the reaction between CO and O on the Pt(1 1 1) surface. The reaction coordinate is defined by the separation between the carbon atom belonging to chemisorbed CO and the isolated oxygen atom chemisorbed initially in the f.c.c. hollow site of the Pt(1 1 1) surface. Several surface atoms are labelled to aid discussions of the reaction pathway.

isolated O atom and the Pt surface. Our analysis of the reaction is based on a partitioning of the total energy amongst these fragments.

In this context the energy partitioning is most efficiently accomplished if we adopt a fragment orbital basis set composed of the molecular orbitals of the individual fragments. By taking advantage of the partitioning of the chemisorption system into geometric fragments, such fragment orbital basis sets afford us the opportunity to formulate our description of the electronic structure in terms of the interactions between the individual molecular orbitals of CO, O, and the surface.

The energy partitioning is formulated in terms of on- and off-fragment Hamilton populations according to

$$E_{tot} = \sum_{\substack{\text{FRAGS} \\ i}} FHP_i + \sum_{\substack{\text{FRAGS} \\ i}} \sum_{\substack{\text{FRAGS} \\ j>i}} FHP_{ij}. \quad (1)$$

The on-fragment Hamilton population for the ith fragment, FHP_i is defined to be the energy contribution due to electron occupancy of the fragment orbitals belonging to the ith fragment. The ijth off-fragment Hamilton population, FHP_{ij} corresponds to the energy of interaction between the fragment orbitals on fragments i and j.

The formulation and use of such energy partitioning schemes within both fragment orbital and atom-localized basis sets is discussed in some considerable detail in a previous paper [3].

By choosing to formulate a partitioning of the total energy according to Eq. (1) we are able to evaluate a measure of surface–CO bonding, which we take to be the off-fragment Hamilton population between the surface and CO fragments, $FHP_{surface–CO}$. We also arrive at a measure of surface–O bonding, $FHP_{surface–O}$ and a measure of the direct (through-space) interaction between coadsorbed CO and O, $FHP_{O–CO}$. These measures are subsequently referred to as the surface–CO, surface–O and OC–O bond Hamilton populations (BHPs).

In addition to the surface–CO, surface–O, and OC–O BHPs we need to consider both the variation in C–O bonding and Pt–Pt bonding within the surface along the reaction coordinate in order to be able to describe the form of the reaction profile calculated by Alavi et al. [4]. Both are strongly influenced by the positions of the adsorbates on the surface.

In order to evaluate the extent of Pt–Pt bonding within the surface fragment we must reformulate the on-fragment Hamilton population for the surface fragment, $FHP_{surface}$ – which is defined to be the contribution to the total energy resulting from electron occupancy of the molecular orbitals belonging to the surface fragment – in terms of an "atom-bond" partitioning. The on-fragment energy is partitioned amongst the atoms and bonds within the surface fragment according to

$$FHP_{surface} \equiv \sum_{\substack{\text{ATOMS} \\ i\epsilon S}} AHP_i + \frac{1}{2} \sum_{\substack{\text{ATOMS} \\ i\epsilon S}} \sum_{\substack{\text{ATOMS} \\ j\epsilon S}} BHP_{ij}, \quad (2)$$

where the set S contains the atoms belonging to the surface fragment.

The atomic Hamilton population (AHP) for the ith atom, AHP_i defines the energy contribution resulting from electron occupancy of the valence basis orbitals associated with the ith atom and the BHP between atoms i and j, BHP_{ij} defines the contribution to the total energy resulting from the interactions between the valence basis functions on atoms i and j.

Thus the Pt–Pt BHP refers to the sum of the BHPs between the atoms belonging to the surface fragment as defined by the second term in Eq. (2). Similarly the C–O BHP is defined to be the sum of the interactions between the valence orbitals of the carbon and oxygen atoms defining the CO fragment.

At various points along the reaction path it proves useful to relate the surface–adsorbate interactions to those for the adsorbate in the absence of a coadsorbate. For instance, a comparative study of surface–CO bonding in frame 1 and surface–CO bonding for a $p(2 \times 2)$ array of CO molecules chemisorbed on the top site of a Pt(1 1 1) surface (Scheme 2) provides insight into the electronic structure perturbations introduced on coadsorbing oxygen on the surface.

To facilitate such comparisons we have calculated the equilibrium chemisorption geometries for CO at one-quarter monolayer coverage on the top

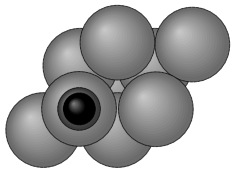

top site

Scheme 2.

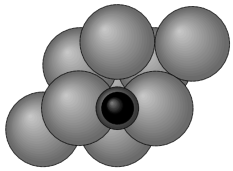

bridge site

Scheme 3.

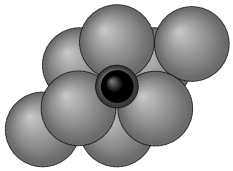

fcc hollow site

Scheme 4.

(Scheme 2) and bridge (Scheme 3), sites of the Pt(1 1 1) surface using the fhi96md density functional package [5]. The chemisorption geometry for quarter layer coverages of oxygen on the bridge (Scheme 3) and f.c.c. hollow (Scheme 4) sites was also calculated. The details of the DFT and tight-binding calculations are left to the appendix.

The CO and O chemisorption geometries obtained from our DFT calculations are summarized in Table 1 and are in excellent agreement with those obtained recently by Bleakley and Hu [6] for $p(2 \times 2)$ coverages of CO and O on the Pt(1 1 1) surface.

3. An overview of CO oxidation on the Pt(1 1 1) surface

Before attempting to explore aspects of the reaction between CO and O in detail, we describe the principal changes in the electronic structure on progressing along the reaction coordinate defined by frames 1–8 in Fig. 1.

We begin by noting that in frame 1, the CO–Pt and O–Pt BHPs are ~1.3% and ~1.0% greater than their respective BHPs calculated for the $p(2 \times 2)$-CO/Pt(1 1 1) and $p(2 \times 2)$-O/Pt(1 1 1) chemisorption systems. The similarity is not surprising, given that the Pt–C, C–O, and Pt–O bond lengths in frame 1 can be reconstructed to within 0.01 Å by superimposing the $p(2 \times 2)$ coverage of O atoms in f.c.c. hollow sites and the $p(2 \times 2)$ coverage of CO chemisorbed on top sites summarized in Table 1. Thus we conclude that coadsorbed CO and O do not interact significantly in frame 1. The apparent short range nature of the interactions between chemisorbed CO and O on the Pt(1 1 1) surface was also pointed out recently by Bleakley and Hu [6].

Frame 2 represents an intermediate step in the transition from CO chemisorption on the top site (frame 1) to CO chemisorption on a bridging site (frame 3). We computed a modest increase in the extended Hückel total energy between frames 1 and 2, consistent with both the 0.5 eV increase in the total energy calculated by Alavi et al. [4] using

Table 1
Summary of the CO/Pt(1 1 1) and O/Pt(1 1 1) chemisorption geometries obtained using the fhi96md plane-wave DFT code

$p(2 \times 2)$-CO/Pt(1 1 1)			$p(2 \times 2)$-O/Pt(1 1 1)	
CO site	Pt–C/Å	C–O/Å	O site	Pt–O/Å
Top	1.86	1.13	Bridge	1.92
Bridge	1.94	1.16	f.c.c. hollow	2.03

plane-wave density functional theory and the experimental preference for top site CO chemisorption [7].

By frame 3, CO has completed its transition to a bridging site whilst oxygen remains chemisorbed in a 3-fold (f.c.c.) hollow site. At 2.02 Å the Pt–C bonds are ~0.08 Å longer than those calculated for the p(2 × 2)-CO/Pt(1 1 1) chemisorption system with CO in the bridging position (Table 1). Thus, not unexpectedly, surface–CO bonding in frame 3 is somewhat reduced relative to that for bridge site chemisorption in the p(2 × 2)-CO/Pt(1 1 1) chemisorption system. The ~12% reduction in the Pt–CO BHP involves reductions in both the σ and π components of the Pt–CO bond.

Further, in frame 3, the Pt–O contact involving the surface Pt atom "shared" with the chemisorbed CO on the bridge site (denoted I in Fig. 1) is approximately 0.16 Å longer than the remaining two Pt–O contacts. At 2.02 Å the Pt–O bonds between the chemisorbed oxygen atom and surface atoms II and III (Fig. 1) are identical to those calculated for the p(2 × 2)-O/Pt(1 1 1) chemisorption system with oxygen chemisorbed in the f.c.c. hollow site (see Table 1). The increase in Pt–O bond length for the bond to Pt I is accompanied by a significant decrease in the Pt–O BHP. We find that the total Pt–O BHP is reduced by ~10% relative to that for the p(2 × 2)-O/Pt(1 1 1) chemisorption system with oxygen in the f.c.c. hollow site. The reduction in the Pt–O BHP is primarily the result of reduced Pt–O orbital interactions involving those oxygen p-orbitals oriented parallel to the plane of the surface and directed towards Pt I. On noting that the Pt–O bond lengths to Pt II and Pt III are essentially unchanged in frame 3 relative to the corresponding bonds in the p(2 × 2)-O/Pt(1 1 1) chemisorption system with oxygen in the fcc hollow site, we consider the ~10% reduction in the total surface–O BHP equivalent to a 30% reduction in the Pt–O bond to Pt I.

As suggested previously by Alavi et al. [4] we propose that the activation of chemisorbed oxygen on proceeding along the reaction coordinate from frame 1 to frame 3 is the result of a competition for the surface electron density in the vicinity of the shared surface atom, Pt I.

In frame 4 CO is once more chemisorbed on a top site, this time on Pt I with a Pt–CO BHP that is essentially identical to that for frame 1. The *deactivation* of CO contrasts the continued activation of oxygen between frames 3 and 4. The deactivation of CO continues between frames 4 and 5, as does the activation of oxygen, however the changes in the Pt–CO and Pt–O BHPs are significantly less than for the transition between frames 3 and 4. The modest ~3% reduction in the Pt–CO BHP between frames 4 and 5 is the result of an equally modest 0.01 Å increase in the Pt–C bond length between frames 4 and 5 and effectively signals the conclusion of the activation phase of the reaction. Chemisorbed oxygen does not move appreciably between frames 4 and 5 (<0.01 Å). Frame 5 is the *transition state* for the reaction [4].

The activation of chemisorbed oxygen between frames 3 and 5 results in an 18% reduction in the Pt–O BHP relative to that for oxygen chemisorbed in a 3-fold (f.c.c.) hollow site in the absence of coadsorbed CO. Thus the activation of chemisorbed oxygen resulting from the transition from hollow site (frame 1) to bridge site (frame 5) chemisorption results in an ~28% reduction in the Pt–O BHP. If we translate this reduction in the Pt–O BHP into an energetic measure of Pt–O bonding based on the oxygen chemisorption energy calculated recently by Bleakley and Hu for the p(2 × 2)-O/Pt(1 1 1) chemisorption system [6], we note that Pt–O bonding is reduced by ~1.25 eV. Thus if we were to assume that the activation phase of the reaction (frames 1 through 5) involved changes solely in Pt–O bonding, we would anticipate a reaction barrier of ~1.25 eV. This is in fairly good agreement with the experimentally determined reaction barrier of ~1 eV [8] and could be used to support the hypothesis that the reaction barrier is principally due to Pt–O bond breaking. However, we note that the Pt–O BHP for oxygen chemisorbed on the bridge site (frame 5) is ~22% lower than that calculated for oxygen chemisorbed on the bridge site in the absence of coadsorbed CO. Indeed the Pt–O BHP for oxygen chemisorbed in the hollow site (frame 3) is within 2% of that calculated for oxygen chemisorption on the bridge site in the absence of CO. Thus coadsorbed CO is by no means an innocent bystander during

the activation phase of the reaction, and we must incorporate the variation in C–O, surface–CO and Pt–Pt bonding within the surface accompanying the activation of oxygen when attempting to define the origin of the reaction barrier.

In the DFT study of Alavi et al. the total energy of the chemisorption system increases by ~1 eV during activation (frames 1 through 5) with 0.6 eV being expended on moving CO from the top site (frame 1) to the bridging site (frame 3). Relatively minor variations in the total energy (<0.05 eV) between frames 4 and 6 herald the end of the activation phase of the reaction and the onset of OC–O bond formation. The majority of the OC–O bond formation process occurs during the transition from frame 6 to frame 7 and results in an ~0.3 eV reduction in the total energy. A further 0.2 eV reduction in the total energy occurs between frames 7 and 8 and is the result of increased OC–O bond formation.

The extended Hückel description of the reaction barrier is given in Fig. 2 and shows a steady increase in the total energy through the first seven frames, encompassing both the activation phase of the reaction (frames 1 through 5) and the initial stages of OC–O bond formation (frames 4 through 6). It is only during the later stages of OC–O bond formation that we note a decrease in the extended Hückel total energy.

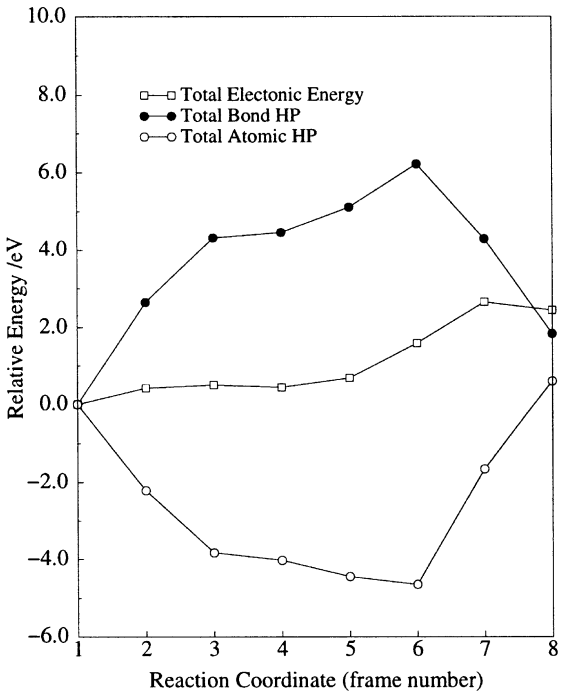

Fig. 2. Total BHP and AHP contributions to the total extended Hückel energy along the reaction coordinate.

In general the total extended Hückel energy is not a reliable energetic measure and our considerable experience with extended Hückel theory prompts us to focus not on the variation in the total extended Hückel energy along the reaction coordinate, but instead the variation in the total BHP during the reaction. The total BHP is obtained from the total extended Hückel energy by combining the off-fragment Hamilton populations defined in Eq. (1) with the "bond contributions" derived from the on-fragment Hamilton populations in a manner analogous to Eq. (2). Thus the total BHP is defined to be the sum of the Pt–CO, Pt–O, OC–O off-fragment Hamilton populations and the BHP contributions to the on-fragment Hamilton populations for the CO and surface fragments.

The remainder of the total extended Hückel energy is comprised of the AHPs for the individual fragments (see Eq. (2)). The AHP's are linearly dependent on the energies of the valence orbitals, which are provided as parameters to the extended Hückel calculation. Thus the total BHP, whose dependence on the energies of the valence orbitals is typically an order of magnitude less than that for the atomic Hamilton populations [3,9], is considerably less prone to changes in the parametrization of the extended Hückel method. We anticipate that on adopting the BHP as a measure of bonding we are minimizing the risk of our reaching conclusions that depend significantly on the parametrization of the extended Hückel method.

The total BHP and AHP are given in Fig. 2. The "mirror image" relation between the total BHP and AHP is, we believe, a characteristic feature of Hamilton population analysis and reflects the transfer of electron density to the atomic centres that occurs in response to a decrease in bonding within the system. Frequently, a relatively minor variation in the extended Hückel total energy re-

sults from the counterbalancing of substantially larger variations in the bond and atomic Hamilton population terms, as noted in recent contributions from our group [10,11].

The variation in the total BHP (Fig. 2) is a more faithful representation of the reaction profile obtained using density functional methods [4], particularly throughout the activation phase and the later stages of OC–O bond formation. This would suggest that the reaction barrier is principally the result of variations in the sum of orbital interactions and is thus amenable to a Hamilton population description. We note however that the continued reduction in the total BHP throughout the initial stages of OC–O bond formation (frames 4 through 6) does not seem to reflect the ~0.05 eV decrease in the total energy calculated by Alavi et al. during the same phase of the reaction.

The failure of the total BHP to reproduce the modest decrease in the total energy noted by Alavi et al. during the initial stages of OC–O bond formation (frames 4 through 6) is an illustration of the consequences of using a qualitative measure of bonding. The variation in the total BHP during the initial stages of OC–O bond formation is the net result of counterbalancing 2.26 and 3.02 eV reductions in the Pt–CO and Pt–O BHPs and a 2.19 eV decrease in the C–O BHP against a 6.34 eV increase in the OC–O BHP. The variation in the sum of the Pt–Pt BHPs within the surface layer is essentially constant throughout this phase of the reaction. In situations such as this, where we are attempting to balance the effects of several sizable bond population changes, we choose to emphasize the individual contributions to the variation in the total BHP and place little importance on interpreting the variation in the total BHP.

The situation during both the activation phase of the reaction (frames 1 through 5) and the later stages of OC–O bond formation (frames 6 through 8) is somewhat different. The activation phase is characterized by significant reductions in both Pt–CO and Pt–O bonding and the variation in the total BHP during the later stages of OC–O bond formation is principally the result of increases in the OC–O BHP. Both cases are distinct from the situation during the onset of OC–O bonding (frames 4 through 6) in that we are not attempting to interpret a variation in the total BHP resulting from a counterbalancing of several sizable terms.

In Section 4 we investigate the origin of the reaction barrier as defined by the variation in the total BHP along the reaction coordinate in Fig. 2.

4. Exploring the reaction barrier

We begin our analysis by considering the variation in the BHP between chemisorbed oxygen and the surface along the reaction coordinate. As shown in Fig. 3 the initial movement of CO from the top site (frame 1) towards the bridging site (frame 2) does not result in a significant variation in the Pt–O BHP. However on reaching the bridge site (frame 3) CO induces a significant decrease in Pt–O bonding as evidenced by an ~2.4 eV decrease in the magnitude of the Pt–O BHP.

The "coactivation" of CO and O that occurs between frames 2 and 3 is followed by continued

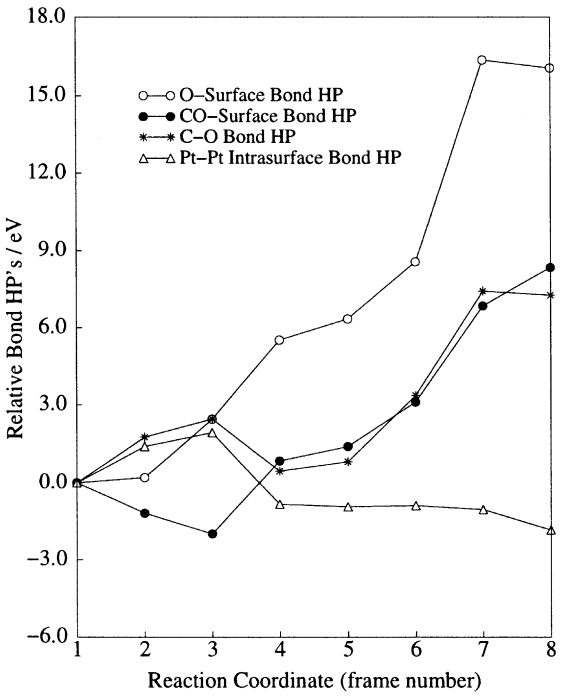

Fig. 3. Surface–CO, surface–O, C–O and Pt–Pt components of the variation in the total BHP along the reaction coordinate.

activation of chemisorbed oxygen equivalent to a further ~3 eV reduction in the Pt–O BHP between frames 3 and 4. Thus the significant decrease in Pt–O bonding between frames 2 and 4 supports the hypothesis that the reaction barrier is due, principally, to a reduction in Pt–O bonding.

If we now turn our attention to the relative Pt–CO, C–O and Pt–Pt BHPs shown in Fig. 3 we note significant variations in all three populations during the initial stages of the reaction. Thus we need consider no less than four contributions in attempting to understand the origins of the reaction barrier.

The transition from top site to bridge site CO chemisorption between frames 1 and 3 results in an ~2 eV increase in the magnitude of the Pt–CO BHP. At first this might seem at odds with the plane-wave DFT results of Alavi et al. [4] which suggest that the transition from top site to bridge site CO chemisorption in the presence of coadsorbed oxygen is endothermic by 0.5 eV. However as noted in our recent study of CO chemisorption on the Pt(1 1 1), Cu(1 1 1), and Al(1 1 1) surfaces [11], it is necessary to consider the net variation in surface–CO bonding, C–O bonding and Pt–Pt bonding within the surface layer when attempting to assess the energetic consequence of moving CO between chemisorption sites. Indeed the ~2 eV reduction in the Pt–Pt BHP within the surface layer and an ~2.5 eV reduction in the C–O BHP between frames 1 and 3 contributes to an overall destabilization by ~2.5 eV in addition to the ~2.4 eV reduction in the Pt–O BHP between frames 1 and 3. In an attempt to effectively separate the CO and O derived contributions to the reaction barrier we choose to combine the variations in surface–CO, C–O and Pt–Pt bonding for frames 1 to 3 into a "CO derived" contribution to the reaction barrier.

In Fig. 4 we have combined the variations in surface–CO and C–O bond populations and plotted the resulting function along the reaction coordinate. The sum of the variations in the surface–CO and C–O bond populations is essentially zero during the first three frames and prompts us to conclude that, in addition to the decrease in Pt–O bonding, only the decrease in Pt–Pt bonding within the surface accompanying the transition

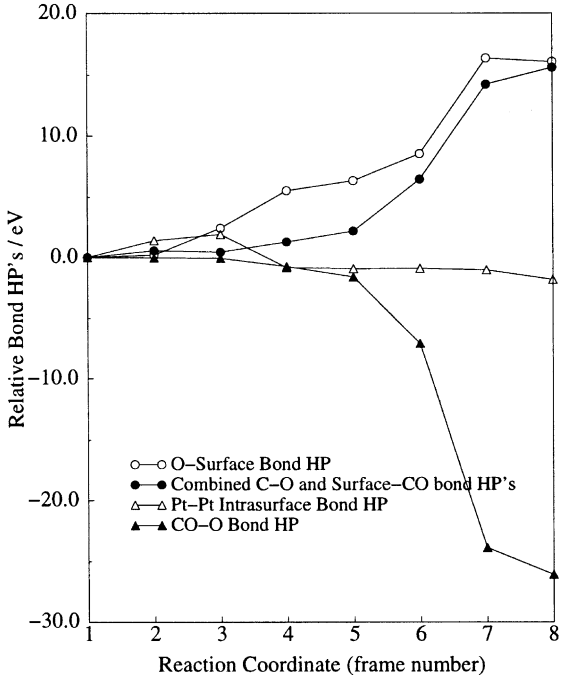

Fig. 4. The variation in the surface–O, OC–O, Pt–Pt and combined surface–CO and C–O BHPs along the reaction coordinate.

from top site to bridge site CO chemisorption contributes significantly to the reaction barrier. We note that the ~2.5 eV decrease in Pt–Pt bonding within the surface layer during the initial stages of the activation phase (frames 1 through 3) is comparable to the ~2.4 eV decrease in Pt–O bonding during this phase of the reaction.

Given that our analysis is, at best, semi-quantitative we will not attempt to construct a quantitative assessment of the origins of the reaction barrier. Instead we conclude that the activation of chemisorbed CO during the initial stages of the reaction, which is in turn directly responsible for the reduction in Pt–Pt bonding within the surface layer, is potentially responsible for a significant portion of the reaction barrier.

The continued activation of chemisorbed oxygen between frames 3 and 5 results in a further reduction in Pt–O bonding and a transition from f.c.c. hollow (Scheme 4) to bridge site (Scheme 3) chemisorption. For oxygen chemisorbed at one-

quarter monolayer coverage on the Pt(1 1 1) surface the transition from f.c.c. hollow site to bridge site chemisorption is accompanied by an increase of ~1.4 eV in the Pt–Pt BHP within the surface layer. This alone cannot be responsible for the ~2.9 eV increase in the Pt–Pt BHP between frames 3 and 5 indicated in Fig. 3. However, the ~1.9 eV increase in Pt–Pt bonding accompanying the transition from bridge to top site CO chemisorption for the one-quarter monolayer coverage of the p(2 × 2)-CO/Pt(1 1 1) chemisorption system [11] is more that adequate to account for the remainder of the the increase in Pt–Pt bonding between frames 3 and 5. Clearly the continued activation of chemisorbed oxygen is also a co-operative phenomenon involving coadsorbed CO.

We conclude this section of our discussion by noting that the ~1.6 eV OC–O BHP developed during the activation phase of the reaction (frames 1 through 5), which in our interpretation corresponds to the direct or through-space interaction between coadsorbed CO and O molecules, is trivial when compared with subsequent contributions to the OC–O BHP totaling ~25 eV from the "bond formation" phase of the reaction (frames 4 through 8). Thus we conclude that the activation phase of the reaction is characterized by an almost entirely surface mediated coactivation of CO and O. As previously noted by Alavi et al. [4] this is, in the present case, a somewhat obvious conclusion given that the OC–O bond length of 2.1 Å in the DFT transition state (frame 5) is much longer than the 1.16 Å bond length observed in molecular CO_2.

Despite the fact that we are using a somewhat qualitative approach to describe the reaction pathway we feel that we have significantly enhanced previous interpretations of the reaction barrier.

5. OC–O bond formation

The coactivation of chemisorbed CO and O depicted in frames 1 through 5 results in the positioning of CO and O on the top and bridging sites immediately surrounding an f.c.c. hollow site. In this section we discuss the electronic structure changes accompanying the various stages of OC–O bond formation in frames 4 through 8.

The restoration of top site CO chemisorption in frame 4 results in a Pt–CO BHP ~5% less than that calculated for top site chemisorption in frame 1. This is consistent with the modest 0.02 Å increase in the Pt–C bond length over that noted in frame 1. In contrast chemisorbed oxygen on the bridge site exhibits a significant reduction in Pt–O BHP of ~18% relative to that calculated for bridge site chemisorption in the p(2 × 2)-O/Pt(1 1 1) chemisorption system. This too is consistent with the 0.08 Å increase in Pt–O bond length in frame 4 relative to that calculated for the p(2 × 2)-O/Pt(1 1 1) chemisorption system (see Table 1).

In an attempt to understand the factors responsible for the significant elongation of the Pt–O bonds in frame 4 we have monitored the Pt–O BHP as a function of the Pt–O bond length in frame 4. On reducing the Pt–O bond length to that calculated for bridge site chemisorption in the p(2 × 2)-O/Pt(1 1 1) chemisorption system (see Table 1) we note that we are able to reproduce the Pt–O BHP calculated in the absence of coadsorbed CO to within 1%. Thus we conclude that the surface electronic structure about the bridging site directly below chemisorbed oxygen is not significantly modified by the presence of coadsorbed CO. This indicates that the principally surface-mediated interaction between coadsorbed CO and O in frames 2 and 3 is no longer in operation and that the significant 0.08 Å increase in the Pt–O bond lengths in frame 4 over those calculated for the p(2 × 2)-O/Pt(1 1 1) chemisorption system with oxygen in the bridge position (see Table 1) is due to the onset of direct (through-space) OC–O bonding.

The lack of through-surface interaction in frame 4 is not that surprising given that the coadsorbed CO and O are no longer occupying chemisorption sites that "share" a common surface atom. Thus we propose that on the Pt(1 1 1) surface – and, potentially, on other close-packed transition metal surfaces – surface-mediated interactions between coadsorbates at low- to moderate coverages are significant only when the chemisorption sites for the coadsorbed species "share" one or more surface atoms.

As illustrated in Fig. 4 the OC–O BHP is essentially zero throughout the initial three frames of the reaction. We interpret the emergence of a 0.74 eV OC–O BHP in frame 4 as the onset of OC–O bond formation via direct through space interactions between the orbitals of coadsorbed CO and O. The OC–O BHP is principally the result of interactions between the CO(2π) band – which is derived from the lowest unoccupied (2π) levels of an isolated CO molecule – and both the oxygen s and p bands. As illustrated in Scheme 5, these interactions involve the donation of electrons from the largely occupied O(s) and O(p) bands to the sparsely occupied CO(2π) bands. At the onset of OC–O bonding in frame 4 the O(s) and O(p) bands are ~93% and 90% full, in contrast to the ~9% filling of the CO(2π) band.

The donation of electron density into the CO(2π) bands is minimal for frame 4, as evidenced by an increase in the occupancy of the CO(2π) bands by 0.5% over that calculated for frame 1. Further, the increased occupancy of the CO(2π) band – which is anti-bonding with respect to the C–O bond as illustrated in Scheme 5 – is not sufficient to cause a notable increase in the calculated C–O bond length.

As we advance along the reaction coordinate from frame 4, the OC–O BHP increases as the OC–O bond forms. Table 2 summarizes the decomposition of the OC–O BHP into the contributions due to the individual CO bands for frames 4 through 8. From Table 2 we note that the interaction between the CO(2π) band and the oxygen s and p bands is the principal energetic driving force towards completion of the reaction during the initial stages of OC–O bond formation (frames 4 through 6). Correspondingly this phase of the reaction is characterized by small but nonetheless significant increases in the C–O bond length as the occupancy of the CO(2π) band increases. The OC–O bond length is significantly reduced during this phase of the reaction, from 2.25 Å in frame 4 to

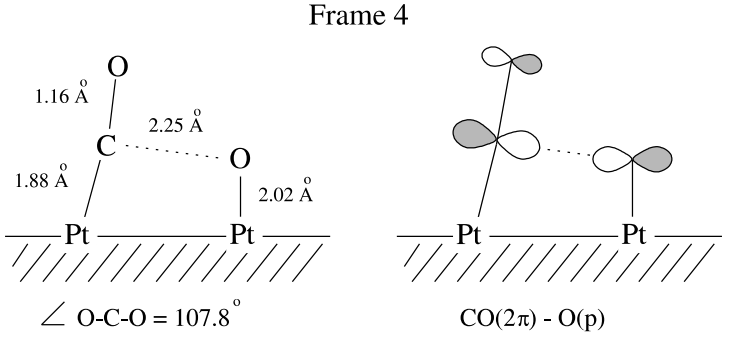

Scheme 5.

Table 2
Decomposition of the OC–O BHP for frames 4 through 8 in terms of the contributions due to the individual CO molecular orbitals[a]

Frame	Total OC–O BHP/eV	3σ	4σ	1π	5σ	2π	6σ
4	−0.74	0.08	0.25	0.23	−0.08	−1.17	−0.04
5	−1.60	0.13	0.37	0.35	−0.27	−2.13	−0.06
6	−7.08	0.34	0.21	0.53	−1.89	−6.17	−0.11
7	−23.88	0.45	−4.74	0.09	−8.01	−11.47	−0.21
8	−26.07	0.44	−5.59	0.12	−9.04	−11.79	−0.20
Molecular CO_2	−37.06	0.32	−9.92	0.92	−17.34	−10.72	−0.31

[a] The molecular orbital contributions to OC–O bonding in molecular CO_2 are also given for comparison.

Table 3
Geometry changes accompanying OC–O bond formation during frames 4 through 8[a]

Frame	Bond length/angle				
	C–O/Å	Pt–C/Å	Pt–O/Å	OC–O/Å	∠O–C–O/°
4	1.16	1.88	2.02	2.25	107.8
5	1.16	1.89	2.02	2.10	109.8
6	1.18	1.94	2.05	1.75	115.5
7	1.22	2.01	2.19,2.33	1.33	129.4
8	1.22	2.05	2.09,2.78	1.30	132.0

[a] For frames 7 and 8 the Pt–O bond lengths for oxygen on the bridging site differ significantly as oxygen becomes increasingly bound to CO and the surface–O bond weakens. Both Pt–O bond lengths are reported for frames 7 and 8.

1.75 Å in frame 6. However at 1.75 Å the OC–O bond is still significantly longer than the C–O bond length of 1.16 Å for molecular CO_2 [12]. The geometric changes accompanying OC–O bond formation during frames 4 through 8 are summarized in Table 3.

We note that the 6.34 eV increase in the OC–O BHP between frames 4 and 6 represents only ~17% of the OC–O BHP for molecular CO_2 (Table 2). Thus we continue to view OC–O bond formation as a perturbation of the Pt–CO and Pt–O chemisorption bonds through frame 6 of the reaction. The large increase in the OC–O BHP between frames 6 and 7 (~16.8 eV) corresponds to an additional 45% of the OC–O BHP calculated for molecular CO_2 and effectively represents the transition from reactants to products on the surface. The significant increase in OC–O bonding is characterized by an ~0.4 Å decrease in the OC–O bond length (see Table 3). The CO_2 geometry from frame 7 is detailed in Table 4 and strongly resembles the structure of the carboxylate moiety in both acetic and formic acids [12]. The acetic and formic acid structures are also summarized in Table 4 for comparison.

Table 4
Summary of the CO_2 chemisorption geometry for frame 7[a]

Species	C–O bond lengths/Å	∠O–C–O/°
Chemisorbed CO_2	1.22, 1.33	129.4
Formic acid	1.20, 1.34	124.3
Acetic acid	1.21, 1.36	122.8

[a] The structures of the carboxylate moieties in formic and acetic acid are also summarized to provide a point of reference.

The ~14° increase in the O–C–O bond angle between frames 6 and 7 represents a substantial step towards the ultimate formation of linear CO_2 and results in a transition from the CO(2π) dominated "side-on" OC–O bonding observed in frames 4 through 6 to a combination of σ and π interactions resembling OC–O bonding in CO_2. The individual contributions of the CO molecular orbitals to OC–O bonding in molecular CO_2 are given in Table 2. The significant increase in the contributions of both the CO(4σ) and CO(5σ) bands is characteristic of the 4σ, 5σ, 2π CO basis used to describe surface–CO bonding on the Pt(1 1 1) surface [11].

The effective transition from reactants to products between frames 6 and 7 is reflected in the form of the total BHP curve in Fig. 2. The significant increase in OC–O bonding between frames 6 and 7 dominates the continued reduction in both Pt–CO and Pt–O bonding resulting in the first increase in the total BHP since the beginning of the reaction.

Continued OC–O bond formation between frames 7 and 8 is somewhat less dramatic than that observed between frames 6 and 7. The continued decrease in the OC–O bond length results in a modest 0.04 Å increase in the Pt–C bond length and the C–O bond length remains unchanged at 1.22 Å. The only noteworthy feature of the transition between frames 7 and 8 is the significant elongation of one of the Pt–O contacts resulting in essentially the transition from bridge to top site oxygen chemisorption. The 0.3 eV decrease in

Pt–O bonding accompanying the transition represents ~5% of the decrease in the Pt–O BHP accompanying the transition from bridge to top site oxygen chemisorption for the p(2 × 2)-O/Pt(1 1 1) chemisorption system and further supports the notion that the oxygen atom is now primarily bonded to the coadsorbed CO and the Pt–O interaction is in essence a perturbation on OC–O bonding.

6. A closer look at how chemisorbed oxygen binds to coadsorbed CO

Thus far we have chosen to view the OC–O bond formation process in terms of the interactions between bands derived from the individual CO molecular orbitals and those arising from both the s and p orbitals on coadsorbed oxygen. In this section we switch our focus and choose to analyse the relative importance of the interactions between chemisorbed CO and the oxygen s and p orbitals.

Table 5 summarizes the components of the OC–O interaction due to the oxygen s and p orbitals for frames 4 through 8. It is clear from Table 5 that both the oxygen s and p orbitals play significant roles in the OC–O bond formation process. We note that although the more diffuse oxygen p orbitals initially dominate the OC–O interaction during the initial stages of OC–O bond formation (frames 4 and 5) the contribution from the oxygen s orbital quickly builds during the later stages of the process. Indeed, we note that after the effective transition from reactants to products between frames 6 and 7 the oxygen s and p orbital contributions to OC–O bonding are comparable in magnitude.

7. Conclusion

To fully appreciate the origins of the reaction barrier in a reaction such as this we believe that it is necessary to maintain a focus on the electronic structure changes occurring within the surface layer in addition to the evolution of surface–adsorbate bonding. By choosing to partition the total electronic energy within an extended Hückel framework we have been able to effectively partition the energy changes occurring during the activation phase of the reaction into CO and O derived contributions. The transparency of this methodology has enabled us to identify a potentially significant "CO-derived" contribution to the reaction barrier in addition to the previously identified contribution arising from Pt–O bond cleavage.

We propose that the initial stages of the reaction involve a surface mediated coactivation of chemisorbed CO and O and that the continued activation of chemisorbed oxygen towards the transition state is aided by an increase in Pt–Pt bonding within the surface layer resulting from the deactivation of CO and the restoration of top site CO chemisorption.

Our "orbital-by-orbital" based analysis of OC–O bond formation effectively highlights the primary role of the CO(2π) band in the early stages of bond formation and the transition from reactants to products on the surface. We also note the im-

Table 5
Oxygen s and p orbital contributions to OC–O bonding[a]

Frame	OC–O BHP/eV	OC–O(s)/eV	OC–O(p)/eV
4	−0.74	−0.05	−0.69
5	−1.60	−0.21	−1.39
6	−7.08	−1.95	−5.13
7	−23.88	−11.92	−11.96
8	−26.07	−13.03	−13.04
Molecular CO_2	−37.06		

[a] The oxygen s and p band contributions to OC–O bonding in molecular CO_2 are given for comparison.

Table 6
Extended Hückel parameters used in this study[a]

Atom	Orbital	H_{ii}/eV	ζ_1	ζ_2	c_1	c_2
Pt	5d	−13.3	6.013	2.696	0.6334	0.5513
	6s	−9.6	2.554			
	6p	−5.6	2.554			
C	2s	−21.4	1.625			
	2p	−11.4	1.625			
O	2s	−32.3	2.275			
	2p	−14.8	2.275			

[a] The coefficients c_1 and c_2 define the contributions of the individual Slater type orbitals in the double zeta expansion used to represent the Pt 5d orbitals.

portance of interactions between the CO orbitals and both the oxygen s and p orbitals during all stages of OC–O bond formation.

In a forthcoming paper we extend our Hamilton population treatment of CO oxidation on the Pt(1 1 1) surface and consider aspects of CO oxidation on both the Rh(1 1 1) and Ru(0 0 0 1) surfaces [13].

Acknowledgements

We are especially grateful to Dr. Peijun Hu of The Queen's University of Belfast for providing us with the atomic coordinates for each of the eight reaction frames and for helpful comments on the manuscript. Without his help this study would not have been possible. We are also grateful to the National Science Foundation for its support of this work by Research grant CHE 99-70089.

Appendix A

The fhi96md density functional package [5] was used to obtain chemisorption geometries for one-quarter monolayer coverages of CO and O on the Pt(1 1 1) surface. The surface was modelled by a two-dimensional slab consisting of three layers of close-packed Pt atoms in the ...ABCABC... stacking obtained by cleaving f.c.c. Pt parallel to the (1 1 1) plane.

The top two layers of the slab were relaxed using a damped Newtonian dynamics scheme [5] prior to CO being placed on the surface. One-quarter monolayer coverages of CO were subsequently placed on the top (Scheme 2) and bridge (Scheme 3) sites of the surface and their geometry optimized. The Pt atoms were not allowed to relax during the CO geometry optimization. Chemisorption geometries for one-quarter monolayer coverages of atomic oxygen in the bridge (Scheme 3) and f.c.c. hollow sites (Scheme 4) were also obtained in this way.

The geometry optimizations were carried out using a $2 \times 2 \times 1$ Monkhorst–Pack k-point set [14] within the Perdew–Zunger parametrization of the local density approximation to exchange and correlation [15]. The valence electron density of both the CO/Pt(1 1 1) and O/Pt(1 1 1) chemisorption systems were represented by plane-wave expansions with an energy cut-off of 60 Ryd. All atoms were represented by soft, norm-conserving pseudopotentials of the Trouillier–Martins type [16] in the fully separable form of Kleinman and Bylander [17].

The tight-binding calculations were performed with the program *bind* [18]. A $4 \times 4 \times 1$ Monkhorst–Pack k-point mesh was used to sample the Brillouin zone and the extended Hückel parameters used for Pt, C and O are summarized in Table 6.

References

[1] J. Wintterlin, S.Völkening, T.V.W. Janssens, T. Zambelli, G. Ertl, Science 278 (1997) 1931.
[2] A. Eichler, J. Hafner, Surf. Sci. 433–435 (1999) 58.
[3] W.V. Glassey, G.A. Papoian, R. Hoffmann, J. Chem. Phys. 111 (1999) 893.

[4] A. Alavi, P. Hu, T. Deutsch, P.L. Silvestrelli, J. Hutter, Phys. Rev. Lett. 80 (1998) 3650.
[5] M. Bockstedte, A. Kley, J. Neugebauer, M. Scheffler, Comp. Phys. Comm. 107 (1997) 187.
[6] K. Bleakley, P. Hu, J. Am. Chem. Soc. 121 (1999) 7644.
[7] H. Steininger, S. Lehwald, H. Ibach, Surf. Sci. 123 (1982) 264.
[8] G. Ertl, Surf. Sci. 299 (1994) 742.
[9] W.V. Glassey, R. Hoffmann, J. Chem. Phys. 113 (2000) 1698.
[10] G.A. Papoian, J.K. Norskov, R. Hoffmann, J. Am. Chem. Soc. 122 (2000) 4129.
[11] W.V. Glassey, R. Hoffmann, submitted for publication.
[12] CRC Handbook of Chemistry and Physics, 80th edition, CRC press.
[13] W.V. Glassey, R. Hoffmann, in preparation.
[14] H.J. Monkhorst, J.D. Pack, Phys. Rev. B 13 (1976) 5188.
[15] J.P. Perdew, A. Zunger, Phys. Rev. B 23 (1981) 5048.
[16] N. Troullier, J.L. Martins, Phys. Rev. B 43 (1991) 1993.
[17] L. Kleinman, D.M. Bylander, Phys. Rev. Lett. 48 (1982) 1425.
[18] G.A. Landrum, W.V. Glassey, BIND (version 3.0), part of the YAeHMOP extended Hückel molecular orbital package available at URL: http://overlap.chem.cornell.edu:8080/yaehmop.html/.